(11) Zhang, M. Y.; Liang, X. Y.; Chen, Y. Y.; Liang, X. G. *Anal. Chem.* **56**, 2288-2290.
(12) Tabet, J. C.; Jablonski, M.; Cotter, R. J.; Hunt, J. E. *Int. J. Mass Spectrom. Ion Processes* **1985**, *65*, 105-107.
(13) Brown, R. S.; Wilkins, C. L. *J. Am. Chem. Soc.* **1986**, *108*, 2447-2448.
(14) Budzikiewicz, H. *The Porphyrins*; Academic Press: New York, 1978; Vol. 3, pp 395-461.
(15) Gallegos, E. J.; Sundararaman, P. *Mass Spectrom. Rev.* **1985**, *4*, 55-85.
(16) Wilkins, C. L.; Weil, D. A.; Yang, C. L. C.; Ijames, C. F. *Anal. Chem.* **1985**, *57*, 520-524.
(17) Brown, R. S.; Wilkins, C. L. 34th Annual Conference on Mass Spectrometry and Allied Topics, Cincinnati, OH, June 8-13, 1986.
(18) Tembruell, R.; Lubman, D. M. *Anal. Chem.* **1986**, *58*, 1299-1303.
(19) Johnson, J. V.; Britton, E. D.; Yost, R. A.; Quirke, J. M. E.; Cuesta, L. L. *Anal. Chem.* **1986**, *58*, 1325-1329.

RECEIVED for review July 16, 1986. Accepted September 10, 1986. Support from the National Institute of Health under Grant GM-30604 is gratefully acknowledged. R.S.B. was partially supported by a grant from the UC, Riverside, Toxic Substances Research and Training Program.

# Square Wave Voltammetry at the Mercury Film Electrode: Theoretical Treatment

**S. P. Kounaves, J. J. O'Dea, P. Chandresekhar,[1] and Janet Osteryoung***

*Department of Chemistry, State University of New York at Buffalo, Buffalo, New York 14214*

**The theoretical response for the application of square wave voltammetry to a reversible system at the mercury film electrode is derived. Numerical calculations using the step method yield voltammograms from which peak heights, shifts, and widths for various values of the thickness parameter are obtained. This method produces results that agree with those of finite difference simulations but is much faster. The differential current voltammograms are symmetrical, shift toward more negative potentials with decreasing film thickness parameter ($\partial nE_p/\partial \log \Lambda = 59.2$ mV), and display a maximum when the diffusion length of the reduced metal in the film equals the film thickness. For customary square-wave parameters of $nE_{sw} = 50$ mV and $n\Delta E_s = 10$ mV the normalized peak height in the thin-film region ($\Delta\psi_p = 1.500$) is larger than that obtained in the thick-film limit ($\Delta\psi_p = 1.312$). Square wave direct voltammetry at mercury film electrodes affords rapid analysis times, discrimination against charging current, enhanced sensitivity, and clear definition of peaks.**

The mercury film electrode (MFE) has gained widespread use as a working electrode in anodic stripping voltammetry (ASV), although more difficult to use than a hanging mercury drop electrode (HMDE), because of its advantages in sensitivity and resolution (*1*). In conjunction with various pulsed waveforms and ASV, it has been used successfully and routinely for trace-metal determinations in a variety of natural samples (*2*). In spite of this it is rarely used directly as a voltammetric electrode.

In cases where the reduced species simply acts as a current carrier, the MFE should behave as any other metal electrode. However, a more interesting case arises when the reduced species is soluble in mercury, i.e.

$$M^{n+} + ne^- = M(Hg) \quad (1)$$

The theory of linear-scan voltammetry for this case has been described by de Vries and van Dalen (*3*, *4*). Subsequently both solution-soluble reactions and reaction 1 were investigated experimentally by Perone and Davenport (*5*). Extensive work, both experimental and theoretical, has been done for cyclic voltammetry for reaction 1 at the MFE by Kublick and coworkers (*6*, *7*). However, these electrodes do not appear to be used routinely for voltammetry, probably because of irreproducibility. It seemed to us that square wave voltammetry in this application would give advantages of increased sensitivity and discrimination against background currents which could make this a practical electrode for routine work. Also, at high effective scan rates the total amount of material converted can be small, thus helping to minimize damage to the film. These points have been demonstrated experimentally (*8*).

If direct voltammetry for reaction 1 could be established as a routine analytical technique, the same experimental system could be used for direct and for anodic stripping voltammetry, thus increasing the practical utility of both. Also, it would permit voltammetric work at mercury electrodes in settings where use of elemental mercury is either discouraged or forbidden. We present here a theoretical treatment of square wave voltammetry at the mercury film electrode. Subsequent papers will deal with square wave anodic stripping voltammetry and with experimental applications of these techniques.

## THEORY

The mathematical treatment of restricted diffusion in thin films is well-developed (*3*, *4*), and the numerical solution of the diffusion equations for the square-wave waveform have been described (*9*). Along with the integral equations already derived by O'Dea (*10*) for SWV with unrestricted diffusion and by Christie and Osteryoung (*11*) for staircase ASV these developments form the basis for the following theoretical treatment.

Figure 1 illustrates the square-wave waveform applied in the direct voltammetry experiment. The characteristic parameters for the waveform are $\Delta E_s$, the step height, $E_{sw}$, the square wave half-peak amplitude, and $\tau$, the square-wave period. Each step is further divided into subintervals of length $d$ to facilitate the calculations described below.

The model used for the mathematical description is shown in Figure 2. We consider a solution of infinite thickness, $y$, containing oxidized species, O, at initial bulk concentration

[1] Present address: Physical Sciences Center, Honeywell, Inc., Bloomington, MN 55420-5601.

0003-2700/86/0358-3199$01.50/0 

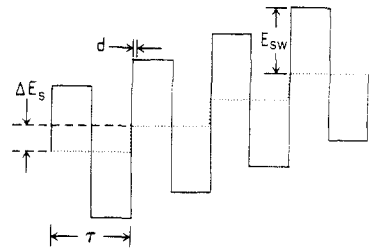


**Figure 1.** Square waveform showing the step height, $\Delta E_s$, square wave amplitude, $E_{sw}$, square wave period, $\tau$, and integration subintervals, $d$.

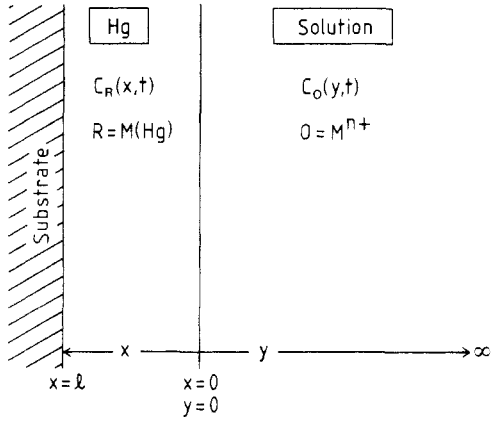


**Figure 2.** Model used for theoretical treatment and numerical calculations.

$C_O^*$, and a thin layer of mercury of thickness $l$ into which a reduced species, R, diffuses until restrcted by the substrate at $x = l$.

We wish to solve the diffusion equations

$$D_O\partial^2 C_O(y, t)/\partial y^2 = \partial C_O(y, t)/\partial t \quad (2)$$

$$D_R\partial^2 C_R(x, t)/\partial x^2 = \partial C_R(x, t)/\partial t \quad (3)$$

with the following initial and boundary conditions:

$$C_O(y, 0) = C_O^*; \quad y \geq 0 \quad (4)$$

$$C_R(x, 0) = 0; \quad l \geq x \geq 0 \quad (5)$$

$$C_O(\infty, t) = C_O^*; \quad t \geq 0 \quad (6)$$

$$C_R(x, t) = 0; \quad t \geq 0, x < 0 \quad (7)$$

$$D_R(\partial C_R/\partial x)_{x=l} = 0; \quad t \geq 0 \quad (8)$$

$$-D_R(\partial C_R/\partial x)_{x=0} = D_O(\partial C_O/\partial y)_{y=0} = i/nFA; \quad t > 0 \quad (9)$$

and the Nernstian equilibrium throughout the experiment

$$D_O^{1/2}C_O(0,t) = \epsilon D_R^{1/2}C_R(0,t) \quad (10)$$

where $\epsilon = \exp[nf(E - E_{1/2})]$, $E_{1/2}$ is the reversible half-wave potential, and $f = F/RT = 38.92$ V$^{-1}$ at 25 °C.

The integral equation for the surface concentration of the oxidized form in solution is given by

$$C_O(0,t) = C_O^* - (1/nFA(\pi D_O)^{1/2})\int_0^t [i(u)/(t - u)^{1/2}]\, du \quad (11)$$

The corresponding equation arising from the restricted diffusion of R in the film is obtained with the aid of the hyperbolic inverse Laplace transform (*12*)

$$L^{-1}[(1/s^{1/2})\coth(l(s/D_R)^{1/2})] = (1/(\pi t)^{1/2})H_3((tD_R)^{1/2}/l) \quad (12)$$

where the kernel function, $H_3$, is given by

$$H_3(a) = 1 + 2\sum_{m=1}^{\infty}\exp(-m^2/a^2) \quad \text{for } a < 1/\pi^{1/2} \quad (13a)$$

$$H_3(a) = a\sqrt{\pi}[1 + 2\sum_{m=1}^{\infty}\exp(-m^2\pi^2a^2)] \quad \text{for } a > 1/\pi^{1/2} \quad (13b)$$

The function $H_3$ is an eta function, selected because of its rapid convergence (*11*) with only three summation terms. Thus, the resulting integral equation for the surface concentration of the reduced form in the mercury is

$$C_R(0, t) = (1/nFA(\pi D_R)^{1/2})\int_0^t [i(u)H_3(a)/(t - u)^{1/2}]du \quad (14)$$

where $a = [D_R(t - u)]^{1/2}/l$. Combining eq 10, 11, and 14 results in the final integral equation for the current,

$$\epsilon\int_0^t [i(u)H_3(a)/(t - u)^{1/2}]du + \int_0^t [i(u)/(t - u)^{1/2}]\, du = nFA(\pi D_O)^{1/2}C_O^* \quad (15)$$

For purposes of numerical computation and to facilitate comparison with the unrestricted diffusion case we define the dimensionless quantities

$$\psi(t) = i(t)(\pi\tau)^{1/2}/nFAD_O^{1/2}C_O^* \quad (16)$$

$$z = t/\tau \quad (17)$$

$$\xi = u/\tau \quad (18)$$

to give a dimensionless integral equation for the current function $\psi(t)$:

$$\epsilon\int_0^z [\psi(\xi)H_3(y^{1/2}/\Lambda)/y^{1/2}]\, d\xi + \int_0^z [\psi(\xi)/y^{1/2}]\, d\xi = \pi \quad (19)$$

where $y = z - \xi$ and $\Lambda = l/(D_R\tau)^{1/2}$ (the dimensionless thickness parameter). Equation 19 can be converted to numerical form, using the step method of Nicholson and Olmstead (*13*), to give

$$\epsilon_m\sum_{i=1}^{m} b_i r_j + \sum_{i=1}^{m} b_i s_j = \pi \quad (20)$$

where $j = m - i + 1$, $r$ is a convolution integral

$$r_j = \int_{d(j-1)}^{dj} [H_3(y^{1/2}/\Lambda)/y^{1/2}]\, dy$$

(which is evaluated by a 10-point Gaussian integration), and $s$ is the sum $s_j = 2d^{1/2}[j^{1/2} - (j - 1)^{1/2}]$. The quantity $d$ is the subinterval of integration and is equal to $1/2K$, where $K$ is the number of intervals in each potential half-step. Thus the period $\tau$ is divided into $2K$ intervals of length $d$ so that no discontinuities of potential are included in the integrations (Figure 1).

The $b_m$th term can be separated out of eq 20 to yield

$$b_m = [1/(\epsilon_m r_1 + s_1)][\pi - \sum_{i=1}^{m-1} b_i(\epsilon_m r_j + s_j)] \quad (21)$$

Equation 21 was translated into an appropriate FORTRAN IV program for calculation of the current function $\psi$. The accuracy depends on the number of subintervals, $K$, used for the calculation. No significant changes in peak parameters were seen for values of $K \geq 14$, and thus all calculations were made with $K = 15$. The calculated response is represented as $\psi$ vs. $n(E - E_{1/2})$ for various values of $\Lambda$.

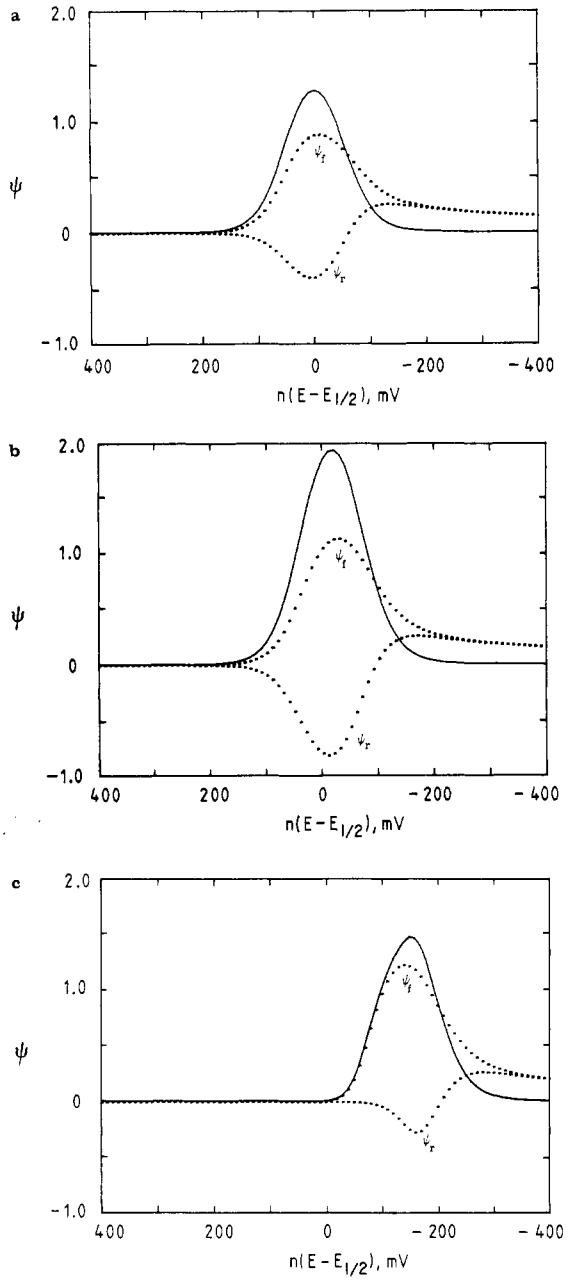


**Figure 3.** Calculated current function voltammograms for forward and reverse (both ···) and net (——) current for $\Lambda$ equal to (a) 100, (b) 1.0, and (c) 0.01; where $\Lambda = l/(D_R\tau)^{1/2}$, $n\Delta E_s$ = 10 mV, and $nE_{sw}$ = 50 mV.

Peak heights and positions were determined from the vertex of the parabolic fit to the three largest dimensionless currents of the voltammogram. Peak widths were defined by tangents to the voltammogram at half-height. The differential current function, $\Delta\psi$, corresponds to the difference between forward and reverse currents and $\Delta\psi_p$ to the peak current.

## RESULTS AND DISCUSSION

Figure 3 shows the general appearance of the calculated dimensionless current–potential voltammograms for three different values of $\Lambda$, using the parameters $n\Delta E_s$ = 10 mV and $nE_{sw}$ = 50 mV. The net current voltammogram retains its symmetrical shape although the individual forward and reverse currents change shape noticeably with decreasing $\Lambda$. The effect of changing $\Lambda$ on the peak height ($\Delta\psi_p$), peak position $n(E_p - E_{1/2})$, and peak width ($nW_{1/2}$) is better shown in Figure 4. Three different regions of behavior are observed. For values of $\Lambda \geq 5$ the peak parameters do not vary and are identical to those for reversible SWV with unrestricted planar

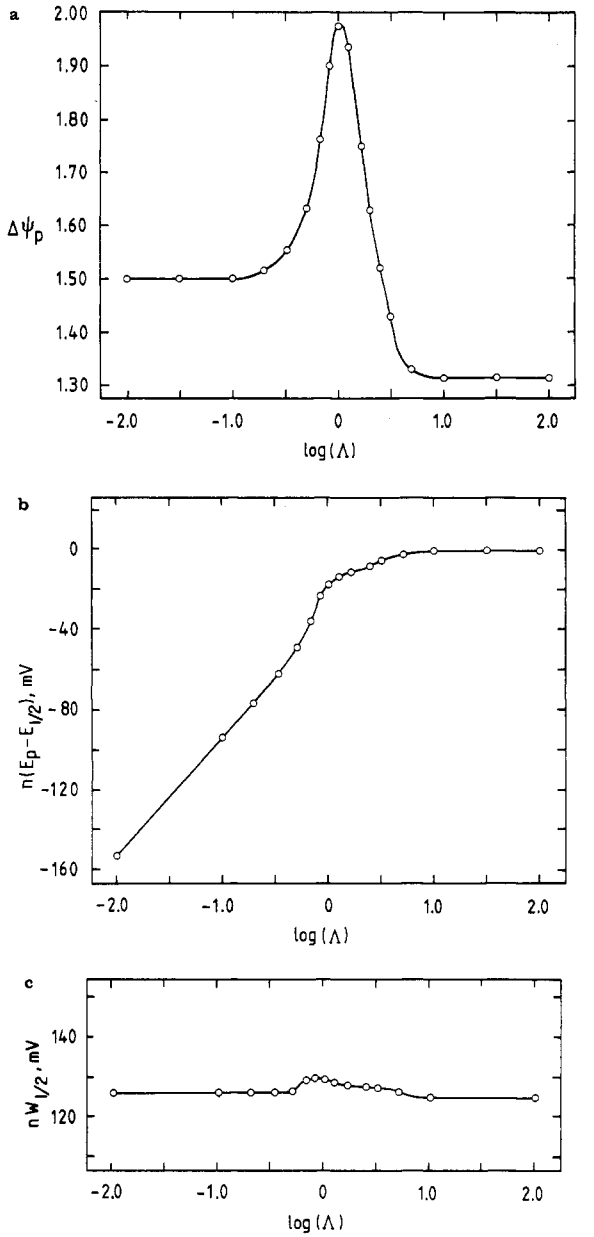


**Figure 4.** Dependence of the (a) current-function peak, $\Delta\psi_p$; (b) peak potential in reference to $E_{1/2}$, $n(E_p - E_{1/2})$; and (c) peak width at half-height, $nW_{1/2}$, on log $\Lambda$ ($n\Delta E_s$ = 10 mV, and $nE_{sw}$ = 50 mV).

diffusion (i.e., $\Delta\psi_p$ = 1.312, $nW_{1/2}$ = 124 mV, and $n(E_p - E_{1/2})$ $\approx$ 0 mV) (9). This is as expected, since eq 19 becomes identical to that for the unrestricted diffusion case (as $l \rightarrow \infty$, $H_3(a) \rightarrow 1$). As one progresses to thinner films the peak shifts only slightly ($\approx$8 mV) toward more negative potentials but dramatically increases in height until a maximum value of $\Delta\psi_p$ is reached at $\Lambda$ = 1. This maximum is caused by an abrupt decrease in $\psi_r$ for $\Lambda < 1$, which causes $\Delta\psi$ to decrease even though $\psi_f$ increases. That is, as the diffusion length in solution at the time of current measurement becomes larger than the film thickness, the flux of O at the electrode surface decreases sharply with decreasing $\Lambda$. A similar phenomenon has been seen with staircase stripping voltammetry (11).

For values of $\Lambda <$ ca. 0.1, $\Delta\psi_p$ (for $n\Delta E_s$ = 10 mV and $nE_s$ = 50 mV) attains a constant value of 1.500 (Figure 4a). This is the limiting case of thin-film behavior, for which no concentration gradients exist in the film on the time scale of the potential-step perturbation, $\tau/2$. The bulk film concentration $C_R^*$ is then determined by the ratio of surface concentrations. This behavior has important analytical consequences, since it predicts that the experimental current for $\Lambda \ll 1$ will be

**Table I. Effect of Square-Wave Amplitude, $nE_{sw}$, on Voltammogram Characteristics[a]**

| $nE_{sw}$, mV | $n(E_p - E_{1/2})$, mV | $nW_{1/2}$ | $\Delta\psi_p$ |
|---|---|---|---|
| 1 | −139 | 87 | 0.136 |
| 5 | −137 | 86 | 0.391 |
| 10 | −138 | 86 | 0.538 |
| 20 | −140 | 88 | 0.917 |
| 50 | −153 | 126 | 1.500 |
| 80 | −176 | 180 | 1.626 |
| 100 | −195 | 219 | 1.648 |

[a] $n\Delta E_s$ = 10 mV, $\Lambda$ = 0.01.

independent of film thickness. This is an exceptionally important attribute which makes routine analysis practical for this system.

The peak shifts to more negative potentials with decreasing values of $\Lambda$, and in the thin film region for $\Lambda < 0.3$, $\partial nE_p/\partial \log \Lambda = 59.2$ mV (25 °C). The peak width is not affected by changes in $\Lambda$, remaining relatively constant ($nW_{1/2} \approx 126 \pm 2$ mV) except around $\Lambda = 1$ (130 mV).

By use of the definition of eq 16, letting $f = 1/\tau$ and $\Delta\psi_p = 1.500$, we can obtain the following expression for the experimental current at a MFE for $\Lambda < 0.1$:

$$\Delta i_p = (8.165 \times 10^4) nAD_O^{1/2} C_O^* f^{1/2} \quad (22)$$

In addition we also have

$$n(E - E_{1/2}) = -34.1 + 59.2 \log \Lambda \text{ mV} \quad (23)$$

and

$$nW_{1/2} = 126.3 \text{ mV} \quad (24)$$

The response is not strongly affected by changes in step height. For example, with $\Lambda = 0.01$ (thin film limit) and $nE_{sw} = 50$ mV, increasing $n\Delta E_s$ from 10 to 40 mV changes the peak position from $-153/n$ to $-148/n$ mV with respect to $E_{1/2}$, the peak width from $126/n$ to $127/n$ mV, and the peak current ($\Delta\psi_p$) from 1.500 to 1.437. Thus, as for unrestricted diffusion, the magnitude of $n\Delta E_s$ has a small effect on the response.

Table I summarizes the effects of varying the square-wave amplitude on the peak parameters in the thin-film region ($\Lambda = 0.01$). With increasing values of $nE_{sw}$, the peak occurs at more negative potentials, as is to be expected, and the peak height increases markedly. This behavior is qualitatively the same as that for unrestricted diffusion. For $nE_{sw} \leq 5$ mV the individual forward and reverse currents have the same sign, so the net current is diminished. For larger values of $nE_{sw}$, the reverse current has the opposite sign (negative for reductions), so the net current is larger than either of the individual currents. For the case of unrestricted diffusion the crossover point occurs at ca. $nE_{sw} = 15$ mV.

From the experimental point of view, it is best to work in the region where $\Delta\psi_p$ is constant ($\Lambda < 0.10$). Under these conditions, film thickness and frequencies routinely attainable yield sensitivities greater than those for the case of unrestricted diffusion.

One would expect that concentrating the product in the film would provide better sensitivity than achievable with unrestricted diffusion. If we examine the ratio of peak currents $\Delta\psi_{(\Lambda<0.1)}/\Delta\psi_{(\Lambda>10)}$ (Figure 4a), we find this ratio is $\approx 1.15$, or concentration in the film produces about a 15% increase in the current. If we could select experimental parameters so that $\Lambda = 1.0$, we would obtain a 50% increase in current. However, reproducibility would be very difficult to achieve since small changes in $\tau$ or $l$ would have pronounced effects on current.

This improvement in signal with concentration in the film contrasts with the qualitative observation that differential pulse ASV (in which the metal ion is replated into the film during the scan) shows about the same sensitivity as linear scan stripping (in which the replating effect does not occur). This point will be discussed more fully in a subsequent paper.

In summary then, direct square wave voltammetry of metals soluble in mercury at the MFE should yield symmetrical differential current voltammograms which shift toward more negative potential with decreasing film thickness parameter, $\Lambda$, and which display increased peak height in the thin-film region with respect to that obtained in the thick-film limit. The range of $\Lambda$ within which enhanced sensitivity can be obtained is easily accessible experimentally. Within that range ($\Lambda < 0.1$) the dimesionless current is independent of $\Lambda$. Thus, SWV in the thin-film region employing thin films and high frequencies should give excellent analytical performance.

## ACKNOWLEDGMENT

We thank Mary Schreiner for her valuable comments and helpful suggestions.

## LITERATURE CITED

(1) Vydra, F.; Stulik, K.; Julakova, E. *Stripping Analysis*; Halsted: New York, 1976.
(2) Nurnberg, H. W. *Anal. Chim. Acta* **1984**, *164*, 1–21.
(3) de Vries, W. T. *J. Electroanal. Chem.* **1965**, *9*, 448–456.
(4) de Vries, W. T.; van Dalen, E. *J. Electroanal. Chem.* **1967**, *14*, 315–327.
(5) Perone, S.; Davenport, K. K. *J. Electroanal. Chem.* **1966**, *12*, 269–276.
(6) Stojek, Z.; Stepnik, B.; Kublick, Z. *J. Electroanal. Chem.* **1976**, *74*, 277–295.
(7) Donten, M.; Stojek, Z.; Kublick, Z. *J. Electroanal. Chem.* **1984**, *163*, 11–21.
(8) Schreiner, M. M.; Osteryoung, J. G. Pittsburgh Conference on Analytical Chemistry, Atlantic City, NJ, March 1984; Abstract 250.
(9) O'Dea, J.; Osteryoung, J.; Osteryoung, R. A. *Anal. Chem.* **1981**, *53*, 695–701.
(10) O'Dea, J. J. Ph.D Dissertation, Colorado State University, Fort Collins, CO, 1979.
(11) Christie, J. H.; Osteryoung, R. A. *Anal. Chem.* **1976**, *48*, 869–872.
(12) *Handbook of Mathematical Functions*; Abramowitz, M., Stegun, I. A., Eds.; National Bureau of Standards: Washington, DC, 1964.
(13) Nicholson, R. S.; Olmstead, M. L. In *Computers in Chemistry and Chemical Instrumentation*; Mattson, J. S., Mark, H. B., McDonald, H. C., Eds.; Marcel Dekker: New York, 1972; Vol. II, Chapter 5.

RECEIVED for review June 11, 1986. Accepted September 8, 1986. This work was supported in part by the National Science Foundation under Grants CHE 8305748 and 8521200.